Green Chemistry

PAPER

View Article Online
View Journal | View Issue

Cite this: *Green Chem.*, 2025, **27**, 14919

Maximizing long-term biohydrogen production with *Clostridium thermocellum* for high solids conversion of lignocellulosic biomass

Young Eun Song, [a,e] Changman Kim, [b] Lydia Rachbauer, [d,e] Lauren R. Magnusson, [c] Chang Dou, [a,e] Katherine J. Chou, [c] Steven W. Singer [d,e] and Eric Sundstrom *[a,e]

Biological hydrogen production from lignocellulosic biomass sustainably couples organic waste reduction with renewable energy generation. Efficient conversion is challenged by the structural complexity of lignocellulose and resulting recalcitrance to enzymatic degradation. *Clostridium thermocellum* natively breaks down biomass with highly effective hemi-/cellulases systems (*i.e.*, cellulosomes) and generates hydrogen in anaerobic cultivation, creating a compelling platform for lignocellulosic biohydrogen production. Achieving commercially viable production rates requires balancing high biomass loading and throughput against uniform mixing conditions required for enzyme dispersion, pH and temperature control, and efficient hydrogen and metabolite removal in continuous operation. To address these barriers to process intensification, we implemented novel reactor and process designs for high-solids lignocellulosic biomass fermentations using the *C. thermocellum* KJC19-9 strain, genetically engineered for co-utilization of cellulose and hemicellulose sugars (*i.e.*, xylose). Via computational fluid dynamics (CFD) modeling and experimental validation, we achieved a >50% improvement in biohydrogen production with an improved anchor-type impeller morphology, coupled to a threefold reduction in agitation rate. To further reduce rheological constraints and accumulation of toxic metabolites, we then transitioned the process to sequencing fed-batch operation. The resulting process generated 24.87 L H_2 L^{-1} from 160 g L^{-1} of deacetylated and mechanically refined (DMR)-pretreated corn stover biomass over 16 days while solubilizing >95% of influent cellulose and hemicellulose, setting a new performance benchmark for continuous production of biohydrogen from lignocellulose.

Received 16th June 2025,
Accepted 9th October 2025

DOI: 10.1039/d5gc03052h

rsc.li/greenchem

Green foundation

1. The scientific literature for biohydrogen production focuses overwhelmingly on short-term batch operation, low solids concentrations, and model feedstocks. This study systematically identifies and address barriers to process intensification – including mixing designs, gas removal conditions, and accumulation of inhibitory metabolites – to develop a batch-continuous biohydrogen production process utilizing real-world biomass feedstocks.
2. This study achieved the highest productivity to date for continuous biohydrogen generation from biomass residuals, generating 24.87 L of hydrogen per L cultivation volume over 16 days of operation, while solubilizing >95% of influent cellulose and hemicellulose.
3. While this work represents a major step forward for intensified biohydrogen production, further research could broaden the impact of this research by reducing or eliminating pretreatment to enable direct use of biomass residuals, eliminating the last remaining technical barrier to distributed deployment.

1. Introduction

The increasing global demand for sustainable energy sources has prompted intensive research into bioenergy technologies, with renewable hydrogen emerging as a compelling bioproduct due to its efficiency as an energy carrier, its flexibility for use across a variety of industrial applications, and its clean-burning nature with no combustion-related CO_2 emissions.[1,2] While hydrogen can be produced *via* a diversity of routes, fossil-based sources accounted for 79% of total production in

[a]*Advanced Biofuel and Bioproducts Process Development Unit, Lawrence Berkeley National Laboratory, Emeryville, CA, 94608, USA. E-mail: esundstrom@lbl.gov*
[b]*Department of Biotechnology and Bioengineering, Chonnam National University, Gwangju 61186, Korea*
[c]*Biosciences Center, National Renewable Energy Laboratory, Golden, CO 80401, USA*
[d]*Joint BioEnergy Institute, 5885 Hollis street, 4th floor, Emeryville, CA, 94608, USA*
[e]*Biological System Engineering Division, Lawrence Berkeley National Laboratory, 1 Cyclotron Road, Berkeley, CA, 94702, USA*

2021, with 62% generated *via* steam methane reforming.[3] To decarbonize the global economy and avert the worst impacts of climate change, hydrogen production must shift fully towards sustainable production modes, including water electrolysis from renewable energy sources and biological production from organic waste materials.[4] Biological hydrogen production, in which biomass is converted to hydrogen and CO_2 by living microorganisms, holds great promise due to its effective de-coupling of the hydrogen and carbon content of biomass, enabling direct integration of hydrogen production with CO_2 sequestration or utilization technologies. Among the biohydrogen production methods, dark fermentation – which can effectively valorize waste lignocellulosic biomass, energy crops, and wet waste streams – is particularly attractive.[5] Dark fermentation offers a number of advantages including simplicity, robustness, and versatility for valorization across the breadth of organic feedstocks.

Clostridium thermocellum, also referred to as *Acetivibrio thermocellus*, is a Gram-positive, rod-shaped, thermophilic bacterium. As a strict anaerobe, it thrives optimally at temperatures between 55 °C and 60 °C. When cultured on cellulosic biomass, *C. thermocellum* natively produces a variety of metabolites including hydrogen, ethanol, lactate, and acetate.[6] This bacterium has a distinct ability to form cellulosomes on the cell surface, anchored on the cell wall or cytoplasmic membrane and housing a variety of hydrolytic enzymes including cellulases, hemicellulases, pectinases, and chitinases. These enzymes work in a coordinated manner to hydrolyze carbohydrate macromolecules, facilitating consolidated bioprocessing (CBP) applications in which saccharification and fermentation occur concurrently and without addition of external enzymes.[7,8] In addition to the cellulosomes, hydrogenases in *C. thermocellum* active in hydrogen generation and mediating cellular redox reactions include three [Fe–Fe] hydrogenases and one [NiFe] hydrogenase.[9–11] These features make *Clostridium thermocellum* a highly flexible single-strain chassis for dark biohydrogen fermentation of lignocellulosic biomass, generating 1–1.65 moles of hydrogen per mole of saccharide dependent on fermentation conditions and the type of biomass utilized,[12] and this strain therefore accounts for the majority of biological hydrogen production research conducted with pure cultures.[13–17] *Clostridium* and related thermophilic strains have been shown to produce hydrogen at yields exceeding 2 mol H_2 mol^{-1} glucose under optimal conditions; however, the majority of published studies achieving high yields from biomass feedstock have utilized biomass hydrolysates, which have been pretreated and saccharified prior to fermentation.[18–20]

Lignocellulosic biomass is primarily composed of 11–50% cellulose (C6-glucose polymer), 6–42% hemicellulose (C5-xylose polymer), and 1–40% lignin, with specific composition dependent on the biomass type.[21] While lignocellulose is a compelling feedstock due to its relatively high sugar content (~70%), low cost, and abundance as a waste resource, commercial-scale fermentation of lignocellulosic biomass for biohydrogen production has proven highly challenging.[22,23] Utilization is primarily challenged by the recalcitrance of the lignin component and by the polymeric bonds in the carbohydrate fraction, which require substantial physical, chemical, or biological pretreatment and saccharification to yield fermentable sugars.[21,24,25] Diminished hydrogen yield has also been noted during biomass fermentation due to metabolic by-products competing for electrons with the hydrogen production pathway,[26] accumulation of inhibitory fermentation by-products,[23] substrate loss during required preprocessing, incomplete utilization of biomass as bacterial growth stops, and heterogeneity in bioreactor during process scale-up.[27,28] Resolving these constraints and enhancing hydrogen yield and productivity in conditions relevant to industrial applications require focused research and development to refine microbial strains, adapt fermentation conditions to real-world feedstocks, and optimize conversion parameters *via* rigorous process engineering.[29,30]

Achieving biomass conversion suitable for commercial deployment necessitates an effective dry substrate concentration of 20% or higher, resulting in significant rheological and materials handling challenges.[31–33] Un-pretreated, milled biomass is the lowest-cost option for feedstock relative to treated biomass, but it typically results in reduced production rates and yields of hydrogen when compared to chemically or thermally pretreated biomass due to increased recalcitrance and occupation of the reactor volume with relatively inert lignin.[34,35] While high solids loading is economically necessary, sugar yields from cellulose and hemicellulose hydrolysis drastically decrease under these conditions due in part to enzyme inhibition resulting from to accumulated soluble components.[31,36–38] Cellulose conversion is also challenged due to poor mixing, resulting in bioreactor "dead zones" featuring uneven pH control, insufficient access to substrate, and insufficient hydrogen removal that leads to in feedback inhibition of biohydrogen production.[39] Development of bioreactors and operational modes optimized for high solids loading (at >15% w/V) and metabolic modifications at both the molecular and physio-ecological levels are therefore required to translate hydrogen yield and productivities achieved under bench-scale conditions towards conditions pertinent to industrial deployment.[29,30] Such systems must also enable continuous hydrogen production, allowing for stable and sustained hydrogen output over time while minimizing cost and downtime associated with cleaning and re-inoculation. End-product inhibition is a primary hurdle to continuous operation, with accumulation of dissolved hydrogen, organic acids, and alcohols inhibiting microbial activity and associated hydrogen yields. Overcoming this inhibitory effect *via* continuous removal of both hydrogen and soluble metabolites is therefore a crucial component of fermentation system design. Long-term or continuous operation has been achieved with model feedstocks, but adaptation of these practices to high intensity fermentation with insoluble, lignocellulosic feedstocks remains a significant challenge.[12,40]

In this study, we utilize computational fluid dynamics and process optimization to model and validate a customized bio-

reactor design for high-solids conversion of pretreated corn stover biomass with *C. thermocellum* strain KJC19-9, genetically engineered for co-utilization of cellulose and a hemicellulose sugars (xylose).[17] This strain was evolved on xylose from an engineered C5-utilizing base strain featuring integrated expression of xylose isomerase and xylose kinase,[41,42] enhancing C5 utilization three-fold. In addition, it incorporates genome-integrated expression of a recombinant beta-xylosidase enzyme from *Thermoanaerobacterium saccharolyticum*, enabling >80% conversion of both glucan and xylan from pretreated biomass in a consolidated bioprocessing configuration. By simulating mixing behavior under variable impeller designs, solids loading conditions, and mixing rates, we develop optimized operating conditions to achieve uniform mixing velocities, eliminate dead zones, and overcome gas transfer limitations. In validation trials, these conditions increase both biomass solubilization efficiency and biohydrogen production *via* dark fermentation. Furthermore, we focus on development of a long-term operational strategy that couples removal of inhibitory soluble metabolites with retention of the biocatalyst. As part of this effort, we address key challenges such as rheology, acetate toxicity, and gas transfer limitations in viscous solutions, developing a stable platform for conversion of lignocellulose to hydrogen over long operational cycles.

2. Materials and methods

2.1. Media and seed cultivation

Clostridium thermocellum KJC 19-9 strains were provided by Katherine Chou at the National Renewable Energy Laboratory (NREL) (see details in SI and Fig. S1).[17] For bacterial reactivation, frozen glycerol stocks were first cultured in CTFUD media containing the following: $Na_3C_6H_5O_7{\cdot}H_2O$, 3 g L^{-1}; $(NH_4)_2SO_4$, 1.3 g L^{-1}; KH_2PO_4, 1.5 g L^{-1}; $CaCl_2H_2O$, 0.13 g L^{-1}; $MgCl_2{\cdot}6H_2O$, 2.6 g L^{-1}; $FeSO_4{\cdot}7H_2O$, 1 mg L^{-1}; MOPS sodium salt, 11.56 g L^{-1}; L-cysteine HCl, 0.5 g L^{-1}; yeast extract, 4.5 g L^{-1}; resazurin solution, 0.5 mg L^{-1}. Pre-culture media for the 2nd seed culture (hereinafter referred as MTC media) contained the following: MOPS sodium salt, 5 g L^{-1}; $Na_3C_6H_5O_7{\cdot}H_2O$, 2 g L^{-1}; K_2HPO_4, 1 g L^{-1}; $C_6H_8O_7{\cdot}H_2O$, 1.25 g L^{-1}; Na_2SO_4, 1 g L^{-1}; $NaHCO_3$, 2.5 g L^{-1}; NH_4Cl, 1.5 g L^{-1}; Urea, 2 g L^{-1}; $MgCl_2{\cdot}6H_2O$, 1 g L^{-1}; $CaCl_2{\cdot}2H_2O$, 0.2 g L^{-1}; $FeSO_4{\cdot}7H_2O$, 1 mg L^{-1}; L-cysteine HCl, 1 g L^{-1}; pyridoxamine dihydrochloride, 20 mg L^{-1}; PABA, 4 mg L^{-1}; D-biotin, 2 mg L^{-1}; vitamin B_{12}, 2 mg L^{-1}; resazurin 0.5 mg L^{-1}. Both media were titrated to pH 7.0 using 2 N NaOH. Both the 1st seed and 2nd pre-culture were transferred and cultivated anaerobically in serum bottles at 60 °C with 5 g L^{-1} (14.6 mM) cellobiose. Cultivation conditions were set at 200 rpm for 24 hours on a rotary shaker (LT-X, Kuhner shaker Inc., USA).

2.2. Simulation

To better understand the velocity field within the bioreactor as a function of solids loading, impeller geometry, and agitation rate, a computational fluid dynamics (CFD) model was designed and used to simulate a variety of operating conditions (M-star CFD, M-Star Simulations LLC, USA). The CFD model was used to predict velocity flux under various biomass loading conditions, with agitation rates ranging from 300 to 500 rpm for the Rushton impeller geometry and 50 to 150 rpm for the Anchor impeller geometry. While gas diffusion and gas hold-up may mildly impact mixing dynamics, it is not presently considered within the bounds of the CFD models.

2.3. Bioreactor initialization & operation

Bioreactor cultivations were performed with 1.40 L media volume and an additional 0.10 L inoculum volume (6.7%), using 2 L jacketed bioreactors equipped with either Rushton (RT) or Anchor (AC)-type impeller geometries (Fig. S2). The OD_{600} at inoculation was adjusted to 0.1–0.15 from the 2nd seed culture. Insoluble biomass substrates utilized for bioreactor fermentations include Avicel PH-101 (cellulose microcrystalline, −50 μm particle size), and pretreated corn stover (DMR-CS). The corn stover was pretreated using the Deacetylation and Mechanical Refining (DMR) process, representing an abundant and widely studied lignocellulosic biomass type. Before pretreatment, the corn stover contained 35.1 ± 4.9% glucan, 19.7 ± 3.9% xylan, and 26.2 ± 1.6% lignin. DMR-CS for the experiments presented was provided by Xiaowen Chen at the National Renewable Energy Laboratory.[43] Initial dry biomass concentrations ranged from 15.0 to 45.0 g L^{-1} Avicel PH-101 and from 26.6 to 79.9 g L^{-1} of DMR-CS (see details in SI 1). Initial DMR-CS concentrations were normalized to match total cellulose concentrations from the equivalent Avicel replicates. Normalization of wet DMR-CS to dry Avicel equivalence was conducted as follows:

$$\text{Dried DMR-CS} = \text{wet DMR-CS} \times \text{DF} \quad (1)$$

$$\text{Total glucose} = \text{dried DMR-CS} \times \text{glucan content}/\text{Hdr} \quad (2)$$

$$\text{Total xylose} = \text{dried DMR-CS} \times \text{xylan content}/\text{Hdr} \quad (3)$$

The drying factor (DF) of approximately 33% was confirmed *via* lyophilization, measured glucan and xylan content were 59.9 ± 4.6% and 17.2 ± 0.4% respectively, dependent on the batch and confirmed *via* biomass compositional analysis at NREL (a representative value of 60% is applied here); and the hydration factor (Hdr) was calculated stoichiometrically by comparing glucan and glucose or xylan and xylose molecular weight (*i.e.*, 0.9 or 0.88) (Table S1).

The Rushton impeller system consisted of a 2 L-size Sartorius bioreactor (Biostat B, Sartorius, USA), equipped with integrated control of pH, gas sparging rate, and temperature. The Anchor impeller system was customized with a pH controller (BL931700, Hanna Instruments, USA), gas sparging system *via* mass flow controller (FMA5520A, Omega, USA), and temperature control *via* a recirculating water bath (Ministat® 125-cc, Huber, Germany). These systems were integrated with agitated 2 L IKA reactors (LR-2.ST, IKA, Germany), and controlled *via* a LabVIEW™ (National instrument, USA) controller

using a data acquisition device (T4, LabJack, USA) (Fig. S3). The agitation speed was set to 100 rpm in the AC and 400 rpm in the RT during the fed-batch operation of both reactors.

In the sequencing (F–S–D–RF) fed-batch operation, the agitation speed was maintained at 100 rpm. Both types of bioreactors, as well as the media and DMR-CS biomass, were sterilized by autoclaving at 121 °C for 15 minutes. Fermentation conditions were maintained at 60 °C and adjusted to maintain pH 7.0 ± 0.05 throughout the fermentation using 2 N NaOH. Pure nitrogen gas was sparged for at least 6 hours at a 500 ml min^{-1} flow rate prior to inoculation to ensure anaerobic conditions. Following inoculation, gas sparging was maintained up to 1.0 vvm (*i.e.* volume of sparged air to volume of liquid per minute), utilizing 30% carbon dioxide with balanced of nitrogen to ensure effective hydrogen removal without stripping inorganic carbon required for biomass production.[39]

2.4. Analysis

For the fermented metabolite analysis, the liquid samples were collected periodically every 24 hours and centrifuged at 13 000 rpm for 2 min. The supernatants were filtered through a centrifugal filter (Nylon membrane, 0.2 μm pore, VWR, USA) at 13 000 rpm for 5 min. The filtered samples were analyzed by high-performance liquid chromatography (HPLC) system (Ultimate 3000, Thermo Fisher Scientific, Waltham, MA) equipped with a refractive index detector and a 300 × 7.8 mm Aminex HPX-87H column (Bio-Rad, Hercules, CA, USA) at 40 °C. The refractive index (RI) and photodiode array (PDA) detector used 4 mM of H_2SO_4 as the mobile phase at a flow rate of 0.4 mL min^{-1}.

For compositional analysis of the final-residual DMR-CS, 50 mL of the final fermentation broth was centrifuged at 4000 rpm for 1 hour. The pellet was washed twice with distilled water to remove any residual sugars and VFAs. Quantitative saccharification of polysaccharides was performed following a scaled-down published protocol (see details in SI 2).[44,45]

Fermentation effluent gases including N_2, CO_2, O_2, and H_2 were monitored in real-time using a magnetic sector MS analyzer (Prima BT Bench Top Process Mass Spectrometer, Thermo Fisher Scientific, Waltham, MA). Off-gas compositional profiles were normalized by off-gas flow rates as calculated in relation to known N_2 inputs to the system to evaluate volumetric hydrogen production rates.

3. Results and discussion

3.1. CFD simulation of solid biomass mixing with variable impeller geometries

Maintenance of homogenous mixing conditions becomes increasingly challenging as the concentration of insoluble biomass substrate rises, resulting in biomass settling, poor gas dispersion due to gas channeling, ineffective pH control, and poor contact between cellulases and unhydrolyzed biomass. These heterogeneities can persist despite increases in agitation and gas sparging due to the formation of persistent dead zones featuring low mixing velocities. The mixing geometry of the system, including the design of the impeller and associated baffles and flow breakers, is therefore a critical parameter in viscous fermentations to ensure efficient hydrogen gas removal, substrate availability, pH control, and inorganic carbon availability within the bioreactor.[39] To predict the mixing behavior of lignocellulosic solid biomass fermentations and better inform our agitation conditions, we developed a computational fluid dynamics (CFD) simulation of the bioreactor to evaluate mixing velocities with variable loadings of raw corn stover biomass (particle density: 1170 kg m^{-3}) across two impeller types – rushton and anchor.[46] Both impeller geometries were investigated across a range of agitation speeds to better evaluate the impact of impeller velocity on mixing.

The six-flat-blade disc turbine, commonly known as the Rushton (RT) impeller, is the most widely recognized and utilized impeller in stirred tank bioreactors (STBR). It propels fluid outward towards the perimeter of the reactor vessel, creating efficient radial flow. The design of its blades makes it particularly suitable for gas–liquid and gas–liquid–solid systems, as it generates high turbulence and excellent mass transfer rates.[47] By contrast, anchor-style (AC) impellers are larger in design and primarily used for mixing viscous pseudo-plastic fluids. In the bioprocess industries, AC impellers are commonly employed in saccharification reactors to hydrolyze high-solids biomass, an application which requires efficient enzyme dispersion and does not necessitate gas–liquid mass transfer. The AC impeller system is designed to induce flow in line with the impeller shaft, termed axial flow (Fig. S2).[48] To investigate the agitation behavior of high-solids solids mixtures based on the impeller type, we considered the influence of stirring speed on mixing behavior.

In Fig. 1, we compare velocity profiles across the bioreactor under different agitation speeds by modeling solid particles representative of milled biomass (*i.e.*, 2.0 mm diameter, 5000 counts). Traditional Rushton impellers are designed for mixing and gas dissolution in aqueous culture, with viscosities near those for pure water. Under high viscosity conditions, only the interior of the vessel is well mixed, leaving substantial unmixed volume around the vessel exterior even when agitation speed is increased to 500 rpm (Fig. 1b). Mixing velocity was high near the impeller with poorly mixed zones around the bioreactor perimeter. Anchor impellers are designed to scrape the full volume of the vessel and operate in tandem with flow breaker to generate turbulence, enabling complete mixing of highly viscous material even with no free water. Due to the wall-scraping impeller system, mixing velocity in this system is therefore highest near the impeller and around the edges of the vessel (Fig. 1a).

To better quantify mixing conditions across the vessel volume, both the max and mean velocities were compared for both impeller types across representative operating conditions (Fig. 1c and d). The maximum velocity of the RT impeller of 2.54 ± 0.07 m s^{-1} was achieved with 500 rpm agitation, with the mean velocity reaching 0.26 ± 0.01 m s^{-1}, approximately 10 times lower than the maximum. The AC impeller showed a sig-

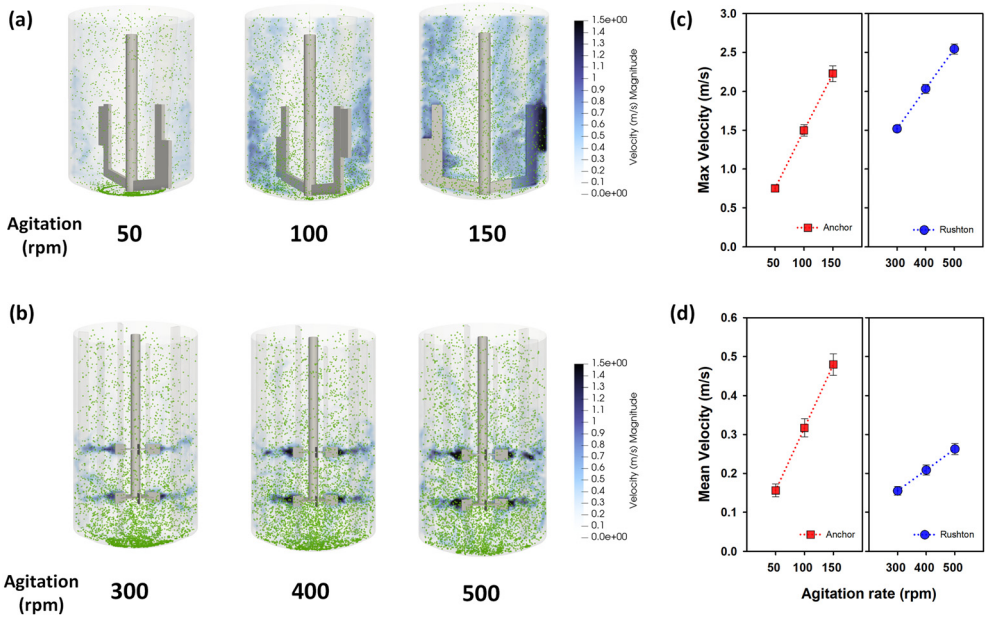

Fig. 1 Comparison of computationally modeled velocity fields between the Rushton and Anchor impellers across variable agitation (rpm) with insoluble DMR corn stover particles (diameter: 2 mm, density: 1170 kg m^{-3}). (a) Anchor impeller, (b) Rushton impeller, (c) Max velocity (m s^{-1}), and (d) Mean velocity (m s^{-1}).

nificant increase in mixing velocity with each 50 rpm increase in agitation, up to a maximum velocity of 2.23 ± 0.10 m s^{-1} under 150 rpm agitation. The mean velocity obtained under this condition was 0.48 ± 0.03 m s^{-1}, 1.85 times higher than the mean velocity for the RT impeller under maximum agitation conditions, indicating significantly more uniform mixing across the reactor volume.

Complete mixing ensures continuous contact between the cellulosome and un-saccharified DMR biomass and improves transport of hydrogen away from microbial cultures, reducing feedback inhibition from hydrogen production. In addition, Kinnarinen *et al.*[49] reported that mixing conditions significantly impact both the glucose yield and the filtration characteristics of hydrolysates after biomass saccharification, resulting in significant savings for solid–liquid separation. In addition to our CFD projections, Kang *et al.*[50] demonstrated that an angle-type impeller – with a similar shape to the modeled anchor impeller – improves the efficiency of simultaneous saccharification and fermentation (SSF) processes at high solid loadings. Based on CFD modeling and literature reports, we therefore predict improved biohydrogen production for the AC impeller during dark fermentation with high-density lignocellulosic biomass as compared to the RT impeller, even at significantly lower agitation speeds.

3.2. Comparison of biohydrogen production from refined insoluble cellulose

Avicel, also known as microcrystalline cellulose (MCC), is a refined form of cellulose known for its relatively facile hydrolysis and bioconversion with *C. thermocellum* when compared to lignocellulosic biomass.[11] Dark fermentation requires strictly anaerobic operation conditions, with anoxic culture conditions typically maintained *via* continuous nitrogen sparging. In this configuration, nitrogen dispersion simultaneously serves to strip hydrogen from the bioreactor. Investigating the metabolic impacts of this system, Kim *et al.*[39] reported that adequate CO_2 supply is necessary to support *C. thermocellum* growth metabolism, with sufficient inorganic carbon necessary to enhance cell growth and maximize hydrogen production. Under conditions with high mixing rates and high rates of hydrogen gas removal, CO_2 supplementation may be necessary to replace stripped inorganic carbon and thereby support cell replication and improved hydrogen production. Optimum sparging rates were investigated, with a sparging condition of 0.5 vvm and approximately 30–35% CO_2 composition determined as the optimum condition; this gas sparging rate was therefore assigned as the default for bioreactor operation in this study (SI section 4 and Fig. S4).

To assess mixing effects with a model feedstock, biohydrogen production was investigated across variable agitation rates and concentrations of Avicel for both the AC and RT impellers (Fig. 2). Hydrogen production yield was compared across multiple experimental campaigns, with Avicel, concentrations from 15.0 to 45.0 g L^{-1} and agitation speeds from 100 to 500 rpm. Hydrogen production was found to increase as a function of both the agitation rate and the Avicel concentration, with the production yield varying distinctly based on impeller geometry. The hydrogen production yield was similar in both impellers under high-speed agitation with lower solids loading, yielding 3.15 ± 0.20 L H_2 L^{-1} culture volume with the AC impeller at 150 rpm and 3.05 ± 0.21 L H_2 L^{-1} with the RT impeller at 500 rpm (Fig. 2a). Reducing agitation to 300 rpm

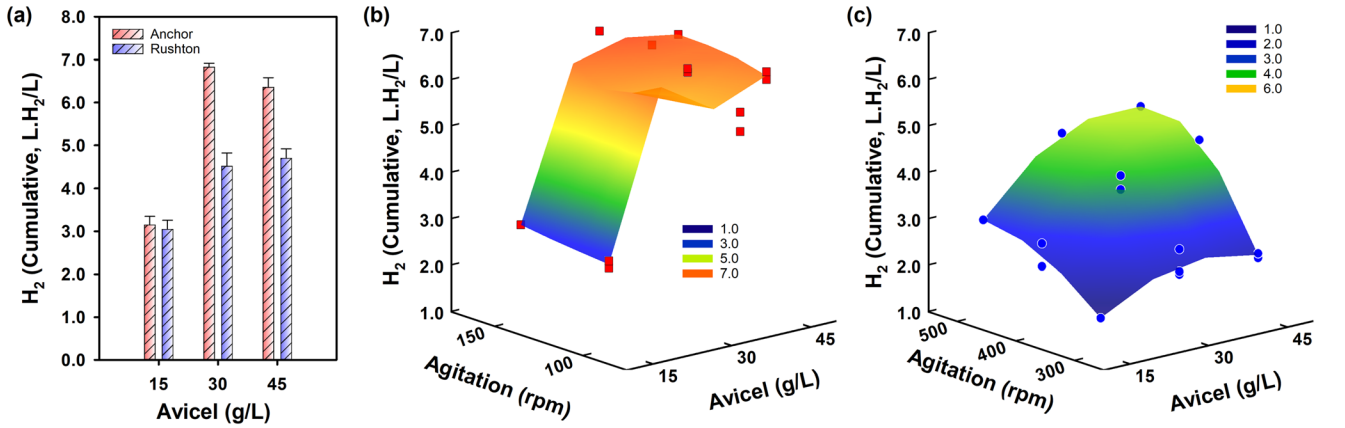

Fig. 2 Comparison of hydrogen production between anchor (at 150 rpm) and Rushton (at 500 rpm) impeller geometries for variable solids loadings of Avicel (a). Heat map of hydrogen production trends with (b) Anchor and (c) Rushton impeller geometries.

with the RT impeller reduced hydrogen production by over 40% to 1.78 ± 0.13 L H_2 L^{-1}. Reducing agitation to 100 rpm in the anchor impeller replicates reduced hydrogen production by less than 10%, indicating better overall mixing performance with the AC impeller under lower velocity mixing conditions (Fig. 2c, Table S2b), as predicted by the average mixing velocities calculated in CFD simulations (Fig. 1).

The effect of impeller morphology was even more apparent under high biomass loading conditions. Hydrogen production increased gradually with agitation and Avicel concentration with the RT impeller up to 4.52 ± 0.30 L H_2 L^{-1} at 30.0 g L^{-1} and 500 rpm, a 50% increase over the 15 g L^{-1} condition. However, the hydrogen yield decreased from 1.627 to 1.202 mol H_2 mol^{-1} glucose, when measured as total equivalent glucose in the Avicel feedstock. This value declined further to 0.818 mol H_2 mol^{-1} glucose at 45 g L^{-1} Avicel loading (Fig. 2a and c, Table S2a). Residual unhydrolyzed Avicel was observed visually after fermentation with both 30 g L^{-1} and 45 g L^{-1} solids loading, reflecting incomplete hydrolysis. The AC impeller's hydrogen production showed a different trend, more than doubling hydrogen production from 3.15 ± 0.20 L H_2 L^{-1} at 15.0 g L^{-1} Avicel to 6.83 ± 0.09 L H_2 L^{-1} at 30.0 g L^{-1} Avicel. In addition, hydrogen yield was maintained, increasingly slightly from 1.672 to 1.726 mol H_2 mol^{-1} glucose, with no residual insoluble Avicel observed at the conclusion of the fermentation. Increasing Avicel loading further to 30 and 45 g L^{-1} decreased the hydrogen yield (Fig. 2a and b, Table S2b). While the system still appears fully mixed under these conditions, decreased hydrogen yield may indicate saturation of the batch reaction due to feedback inhibition resulting from accumulation of dissolved hydrogen or soluble metabolites (Fig. S5). Overall, these results demonstrate that hydrogen production is highly influenced by impeller morphology and mixing rates, with the AC impeller improving mixing conditions and overall hydrogen production at higher solids loadings substantially over the RT impeller as predicted by the CFD simulation.

3.3. Biohydrogen production from pretreated biomass in high solids fermentation

As compared to pure cellulose, bioconversion of lignocellulosic biomass is challenged by additional complexities including the presence of lignin, hemicellulose, and other recalcitrant materials. To assess mixing performance with real-world feedstocks, we therefore transitioned from Avicel feedstock to evaluation of biomass feedstocks under the same mixing conditions employed in Fig. 2. Chemical or physical pretreatment can enhance lignocellulosic biomass conversion by solubilizing lignin and facilitating access of cellulases and hemicellulases to the biomass matrix. The deacetylation and mechanical refining (DMR) pretreatment process is a well-characterized and widely deployed pretreatment technology that generates minimal toxicity for most downstream conversion hosts – this process was therefore utilized to provide representative feedstock for this study.[43] Hydrogen production was compared for variable DMR-CS concentrations up to approximately 80 g L^{-1} dried biomass weight in both the RT and AC impeller configurations. DMR-CS loading was calculated to match the total cellulose concentrations for Avicel trials as shown in Fig. 2. Note that the overall solids loading in these reactors must be significantly higher to achieve equivalence for cellulose, underscoring the rheological challenges associated with lignocellulosic feedstocks.

As shown in Fig. 3, there is a distinct effect on hydrogen productivity across all conditions when comparing the RT and AC impellers, with the AC impeller providing superior mixing, confirming the predictions of the CFD simulation. In the AC impeller fermentation, the maximum total hydrogen production achieved was 4.37 ± 0.50 L H_2 L^{-1} at 150 rpm using 53.3 g L^{-1} DMR-CS, with a maximum hydrogen yield of 0.905 mol H_2 mol^{-1} total sugars, significantly lower than the maximum yield achieved with Avicel. At a lower solids loading of 26.6 g L^{-1} DMR-CS, containing the same glucose content as 15 g L^{-1} Avicel, the total hydrogen produced was 4.27 ± 0.06 L H_2 L^{-1}, 135.5% of the equivalent Avicel condition. As the

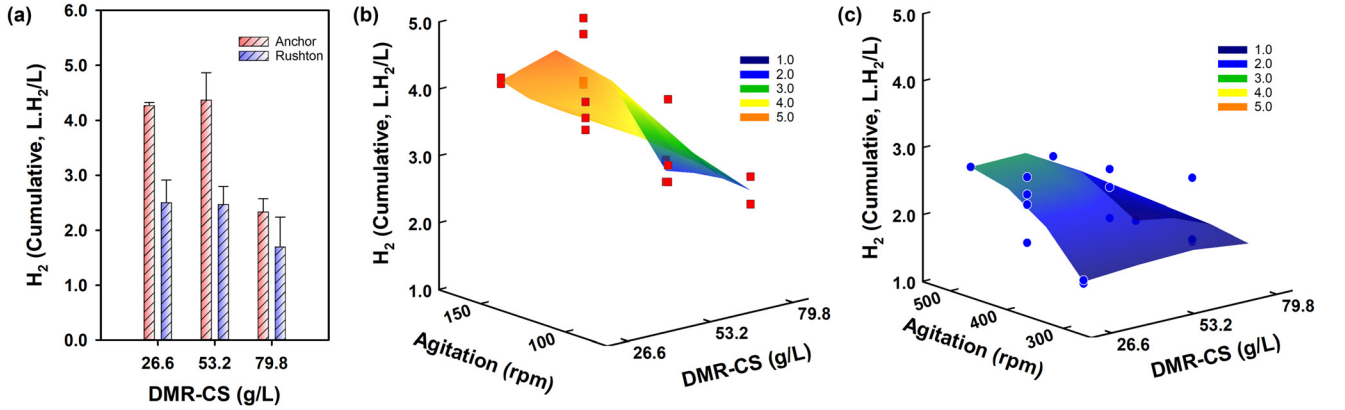

Fig. 3 Comparison of hydrogen production between anchor (at 150 rpm) and Rushton (at 500 rpm) impeller geometries for variable solids loadings of DMR-CS (a). Heat map of hydrogen production trends with (b) Anchor and (c) Rushton impeller geometries.

solids loadings were normalized to equivalent C6 sugar concentrations, this result is likely attributable to xylan utilization with the engineered strain KJC 19-9. Hydrogen yield per total sugar equivalent under these conditions was 1.612 mol H_2 mol^{-1}, nearly matching the best yields achieved with Avicel. Further increasing DMR-CS loading decreased hydrogen significantly to 2.34 ± 0.23 L H_2 L^{-1} at 79.8 g L^{-1} DMR-CS with a yield of 0.319 mol H_2 mol^{-1} total sugars (Fig. 3a and b, and Table S3b). The significant decline in hydrogen yield as a function of solids loading with DMR-CS suggest that for biomass concentrations beyond a certain threshold, viscosity increases negatively impact mixing conditions and associated hydrogen production even with the AC impeller geometry. This impact is exacerbated for DMR-CS conditions as compared to Avicel due to the increased solids loading required to match equivalent C6 sugar concentrations. Hydrogen production with the RT impeller geometry displayed an overall decrease across all conditions when compared to Avicel and when compared to the equivalent AC impeller conditions. As with the AC impeller, the production trend showed a negative impact of increased solids loading on hydrogen production (Fig. 3a and c, and Table S3). Channeling was observed under high-loading conditions, with the bulk biomass accounting for approximately 40% of the total working volume (Fig. S6).

Cellulosic substrates generally have low density and strong hygroscopicity, becoming increasingly paste-like and difficult to handle at solids concentrations approaching or exceeding 15 wt%.[51] Due to low bulk density of milled biomass, the highest DMR-CS concentrations evaluated in batch fermentation (80 g L^{-1}) occupy approximately 45% of the reactor volume, forming a viscous slurry when batched with fermentation media (Fig. S6). Therefore, while the RT impeller may provide sufficient mixing by increasing the agitation speed with soluble substrates and viscosities near those of water, high concentrations of DMR corn stover biomass challenge mixing due to the narrow range of effective agitation. Consequently, although the AC impeller improved hydrogen production significantly when compared to the RT impeller, hydrolysis with *C. thermocellum* KJC 19-9 was ultimately hindered at high solids loading with both impeller geometries, limiting cumulative hydrogen production to levels lower than those observed with equivalent loadings of Avicel.

3.4. Effect of mixing conditions on biomass solubilization

DMR-CS was successfully hydrolyzed and metabolized to hydrogen with *C. thermocellum* KJC 19-9 in both impeller configurations, with significant differences in both yield and total production. To elucidate the core drivers underlying differences between the two impellers, we next examined total solubilization of DMR-CS to better characterize hydrolysis efficiency and its correlation with hydrogen production. Total biomass solubilization was compared for 26.6 g L^{-1} (*i.e.*, low concentration) and 79.8 g L^{-1} (*i.e.*, high concentration) DMR-CS across both impeller types. Changes in the composition of residual biomass were also analyzed to assess hydrolysis efficiency for both glucan and xylan (Fig. 4a and b, and S7).

With an initial solids loading of 26.6 g L^{-1} DMR-CS, total biomass solubilization of 21.1 g L^{-1} was achieved with the AC impeller as compared to 16.6 g L^{-1} with the RT impeller. Total solids solubilization rates were 79.6% and 62.5%, respectively, for the two impeller types. This difference in solubilization efficiency was driven almost entirely by higher residual glucan and xylan in the RT geometry, indicating lower overall hydrolysis efficiency due to ineffective mixing. Under the highest solids loading condition, total solubilization of biomass increased from 21.1 g L^{-1} to 24.6 g L^{-1} in the anchor impeller system, representing a <20% increase in biomass solubilization despite a 3-fold increase in DMR-CS loading, from 26.6 to 79.8 g L^{-1} (Fig. 4a and b, S7, Table S4). While the anchor geometry again resulted in enhanced biomass solubilization efficiency, increasing solids loading clearly resulted in diminishing returns with regard to biomass solubilization and hydrogen yields. This finding is consistent with previous studies reporting diminishing ethanol yields beyond 15 wt% solids, even in simultaneous saccharification and fermenta-

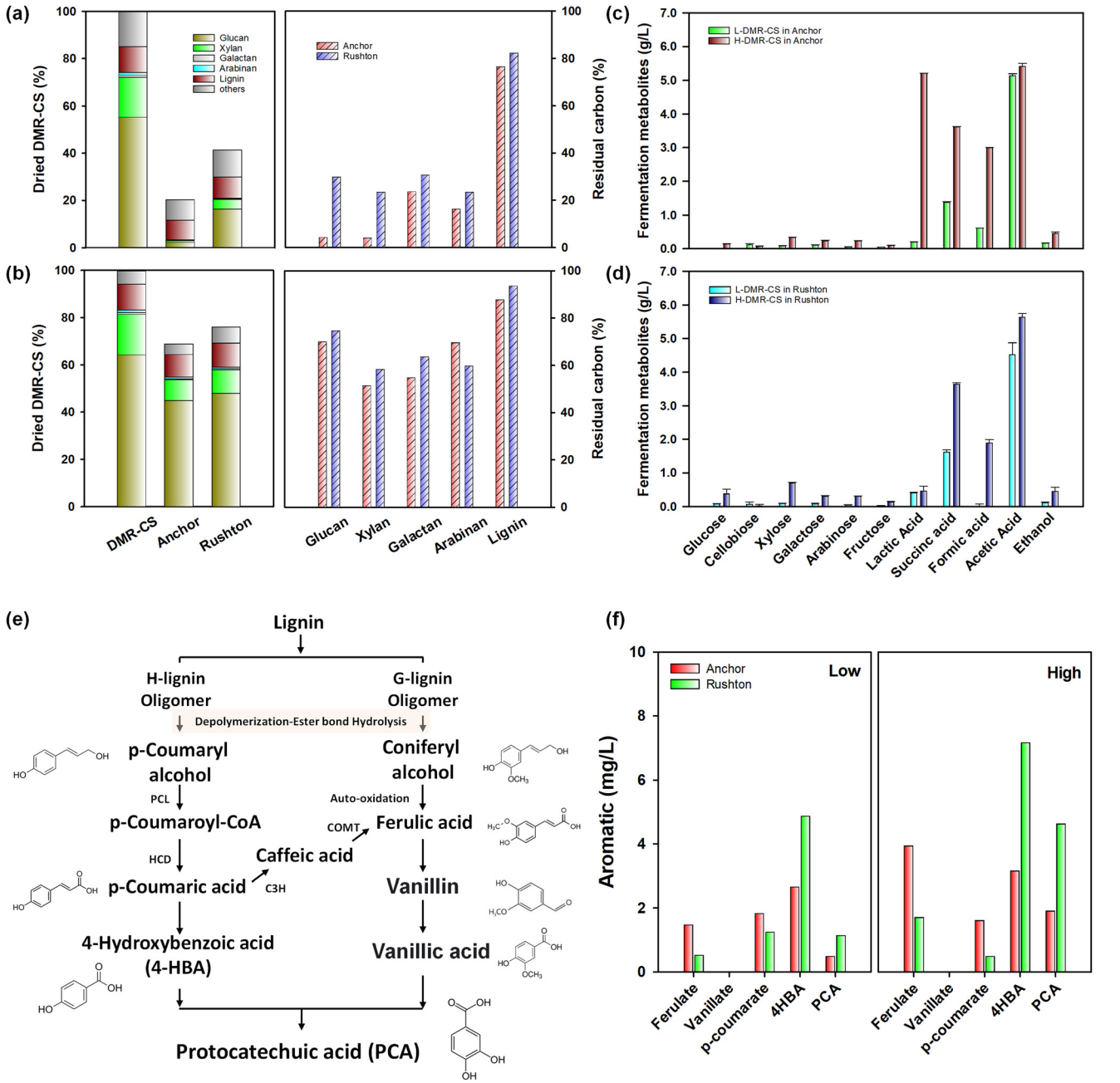

Fig. 4 Comparison of residual biomass following hydrolysis for the Anchor (at 150 rpm) and Rushton (at 500 rpm) impeller geometries across two solids loading conditions: (a) low solids (26.6 g L^{-1} dry DMR-CS) and (b) high solids (79.8 g L^{-1} DMR-CS). Metablite production is shown for (c) Rushton impeller (400 rpm agitation) and (d) Anchor impeller (100 rpm agitation) under high and low DMR-CS concentrations. Pathways for conversion of lignin oligomers into protocatechuate are shown at bottom left (e), with measured aromatic monomer production at bottom right (f).

tion (SSF) processes where external enzymes are supplemented.[52–54] This effect is predominantly attributed to rheological inhibition of biomass hydrolysis and resulting starvation of cell cultures. For biohydrogen production, we observe similar inhibition at DMR-CS concentrations well below this 15 wt% threshold. Reduced performance at 5 to 8 wt% indicates even greater sensitivity to mixing conditions for consolidated bioprocessing configurations requiring continuous hydrolysis to support cellulosome production and continuous gas sweeping to avoid feedback inhibition from accumulated hydrogen.

In the low-biomass loading condition with 14.65 g L^{-1} glucan, 4.50 g L^{-1} xylan, total solubilized glucan and xylan equaled 14.00 g L^{-1} and 4.32 g L^{-1} for the AC impeller, and 10.27 g L^{-1} and 3.45 g L^{-1} for the RT impeller, respectively (Fig. S7 and Table S5). Residual monomeric sugars were below 0.1 g L^{-1} for both impellers, indicating over 99% glucan and over 97% xylan consumption from the hydrolyzed biomass. At

high biomass loading, total solubilized glucan and xylan reached 15.37 g L^{-1} and 6.57 g L^{-1} in the AC impeller, as compared to 13.00 g L^{-1} and 5.62 g L^{-1} with the RT impeller. Residual sugars were slightly higher with higher solids loading, ranging from 0.1 to 0.7 g L^{-1}. Sugar utilization did vary as a function of impeller geometry at high solids loading, with 99% and 95% consumption of glucan and xylan observed with the anchor impeller as compared to 97% and 87% with the Rushton impeller. Low residual sugar concentrations implicate availability of monomeric sugars as a primary bottleneck for biomass conversion, with *C. thermocellum* KJC 19-9 utilizing nearly all available monomeric glucose and xylose under the conditions tested. However, impeller geometry does appear to impact monomeric sugar utilization as a secondary effect, particularly for the introduced xylose utilization pathway under the most challenging mixing conditions. Differences between the AC and RT impellers were also observed in the soluble metabolite analysis (Fig. 4c and d). Under high biomass loading conditions we observe 5.21 ± 0.02 g L^{-1} in lactate production – more than an 11-fold increase for the AC impeller as compared to the RT impeller replicates. Formate was also observed at higher levels with the AC impeller geometry at both high and low solids loading. Accumulation of formate under anaerobic conditions relates to activity of pyruvate formate-lyase, which catalyzes the conversion of pyruvate into formate and acetyl–CoA.[55] When hydrogen is no longer available as an electron acceptor for the reduced ferredoxin produced by pyruvate, less efficient pathways are induced. Thus, formate export *via* pyruvate formate-lyase increases in place of acetyl–CoA production through ferredoxin oxidoreductase.[56] Notably, this shift is associated with increased pyruvate accumulation rather than heightened ferredoxin oxidoreductase activity.

Succinate production was observed at similar levels across both impeller geometries and at both low and high solids loading. Under anaerobic conditions, in *Clostridium thermocellum* and most natural succinate producers phosphoenolpyruvate (PEP) is reported to convert carboxylate *via* PEP carboxykinase (PEPCK) to oxaloacetate (OAA). OAA is then sequentially converted to succinate through malate dehydrogenase (MDH), fumarate hydratase (FH), and fumarate reductase (FR) *via* the reductive TCA pathway.[57,58] Because succinate production may provide the NAD^+ regeneration required by the bacteria, demand for other NAD^+ regeneration pathways is reduced (*e.g.*, production of lactic acids and ethanol), leading to low ethanol and lactate production. Therefore, as the succinate producing metabolic pathway likely branches from oxaloacetate upstream of pyruvate, production of succinate suggests overflow metabolism as a result of high substrate loading, with the bacteria alleviating high carbon flux in upper glycolytic pathway before even reaching pyruvate.

In addition to soluble metabolites, we quantified differences in the concentration of soluble, aromatic monomers derived from biomass deconstruction (Fig. 4f). As a complex and recalcitrant polymer in plant biomass, lignin can significantly influence dark fermentation *via* release of compounds inhibiting microbial activity. Analysis of lignin-derived aromatics can serve as a valuable proxy for overall lignin solubilization activity. H-lignin (*p*-hydroxyphenyl lignin) and G-lignin (guaiacyl lignin) oligomers are linked to hemicellulose through monomers such as *p*-coumaryl alcohol and coniferyl alcohol. These linkages are hydrolyzed by esterase enzymes, such as feruloyl esterase or coumarate esterase, which cleave the lignin–hemicellulose bonds.[59] To quantify the presence of solubilized aromatic lignin monomers we evaluated conversion into protocatechuic acid (PCA), a key intermediate in the lignin degradation pathway (Fig. 4e).

In Fig. 4f, *p*-coumaric acid was detected under all conditions. *p*-Coumaryl alcohol, an H-lignin monomer, can undergo either a CoA-dependent β-oxidation pathway or a non-β-oxidation pathway to form *p*-coumaric acid, typically under aerobic conditions.[60] However, in *C. thermocellum* under anaerobic conditions, *p*-coumaryl alcohol appears to be converted to *p*-coumaric acid through an alternative pathway involving *p*-coumaroyl–CoA ligase (PCL) and hydroxycinnamate decarboxylase (HCD).[61] Ferulate was also detected; ferulate can be formed through the auto-oxidation of coniferyl alcohol as a G-lignin monomer, or could be produced through the actions of *p*-coumarate 3-hydroxylase (C3H) and caffeic acid *O*-methyltransferase (COMT) enzymes from *p*-coumaric acid[62] (Fig. 4e).

As a result, analysis of the H-lignin and G-lignin monomers displayed *p*-coumaric acid and ferulic acid in all conditions. Given that both *p*-coumarate and 4-hydroxybenzoic acid (4-HBA) were obtained, and given the absence of vanillic acid, it can be inferred that protocatechuic acid (PCA) was derived from degradation of H-lignin. Degradation by *C. thermocellum* therefore appears more robust for H-lignin than G-lignin, although the total amounts solubilized were low for both types, suggesting that degradation is not straightforward or that higher solubility constituents were preferentially removed during DMR pretreatment. As with carbohydrate solubilization, differences in degradation reflect increased physical mixing efficiency with the AC impeller, resulting in overall higher solubilization of lignin-derived aromatics.

3.5. Fed-batch operation

At low solids loading and the AC impeller geometry, biohydrogen production yields with DMR-CS exceeded performance with Avicel when normalized to cellulose loading, due in part to utilization of hemicellulose. As solids loading increased, biohydrogen production with DMR-CS drops off more quickly than equivalent Avicel performance, implicating either poor mixing conditions with biomass feedstocks or release of inhibitory compounds from the corn stover biomass. To disentangle these effects we investigated fed-batch operation as an alternative operating mode, with gradual saccharification serving to facilitate enhanced mixing throughout the conversion process. Two conditions were evaluated, each with 35.0 g L^{-1} initial solids loading and three daily bolus additions of 25.0 g L^{-1} each, or 36.7 g L^{-1} each in the high solids condition. When compared to batch performance at 79.8 g L^{-1} total solids, fed-batch operation improved total hydrogen pro-

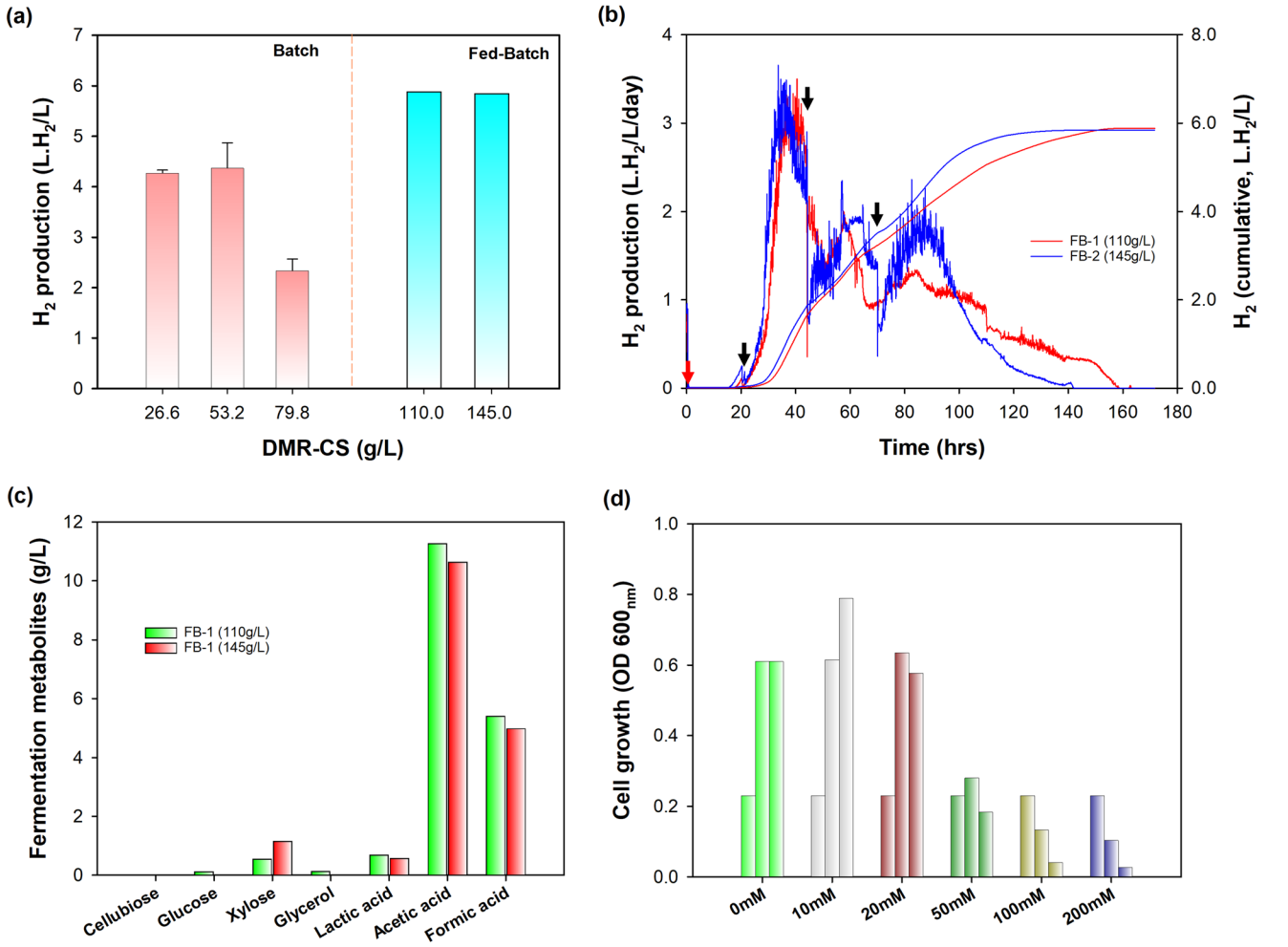

Fig. 5 Comparison of end-point hydrogen production between batch and fed-batch operation (a). Hydrogen production trends for different feed concentrations in fed-batch operation (b). Red arrows indicate initial addition of 35 g L^{-1} of biomass, black arrow indicate subsequent bolus additions of biomass: 25 g L^{-1} (FB-1), and 36.7 g L^{-1} (FB-2). Fermentation metabolite analysis (c). Effect of the acetic acid toxicity for the cell growth (0, 24, 48 h) (d).

duction by a factor of 2.4, to nearly 6 L H_2 L^{-1} (Fig. 5a). This effect confirms mixing as the primary bottleneck for high-solids biohydrogen production in batch fermentation, as continuous biomass hydrolysis reduces the apparent viscosity and thereby reverses the observed trend towards lower performance at higher solids concentrations.

While fed-batch operation is clearly preferable to batch operation at higher solids loading, overall hydrogen production and maximum production rates were similar with both smaller bolus additions (25 g L^{-1}) and larger bolus additions (36.7 g L^{-1}) of DMR-CS (Fig. 5b). When fermentation metabolites were analyzed from these conditions, both acetic acid (over 10 g L^{-1}) and formic acid (over 5 g L^{-1}): were found at concentrations exceeding 100 mM (Fig. 5c). High concentrations of accumulated acetate can affect microbial growth and hydrogen production,[63] with our own analysis of growth impacts indicating substantial acetate toxicity at concentrations of 50 mM and above (Fig. 5d, S8). Consequently, the substantial accumulation of acetate and formate observed in fed-batch operation likely inhibited microbial growth and suppressed hydrogen production. We note that total hydrogen production in fed-batch conditions was similar to maximum hydrogen production observed with Avicel feedstock in batch conditions, indicating that optimal mixing is a necessary prerequisite for maximizing biohydrogen titers but that associated acetate production effectively caps hydrogen titers in both batch and fed-batch operation. To achieve high rates of continuous hydrogen production, it is therefore essential not only to control biomass supply but also to manage the accumulation of organic acids *via* continuous removal, ensuring that inhibitory effects on microbial growth are minimized and enabling sustained long-term hydrogen production.

3.6. Sequencing fed-batch operation

To overcome acetate accumulation and facilitate long-term operation, we developed and evaluated the ferment–settle–drain–refill (F–S–D–RF) sequencing fed-batch strategy for solid biomass fermentation (Fig. 6b, details in SI). The F–S–D–RF

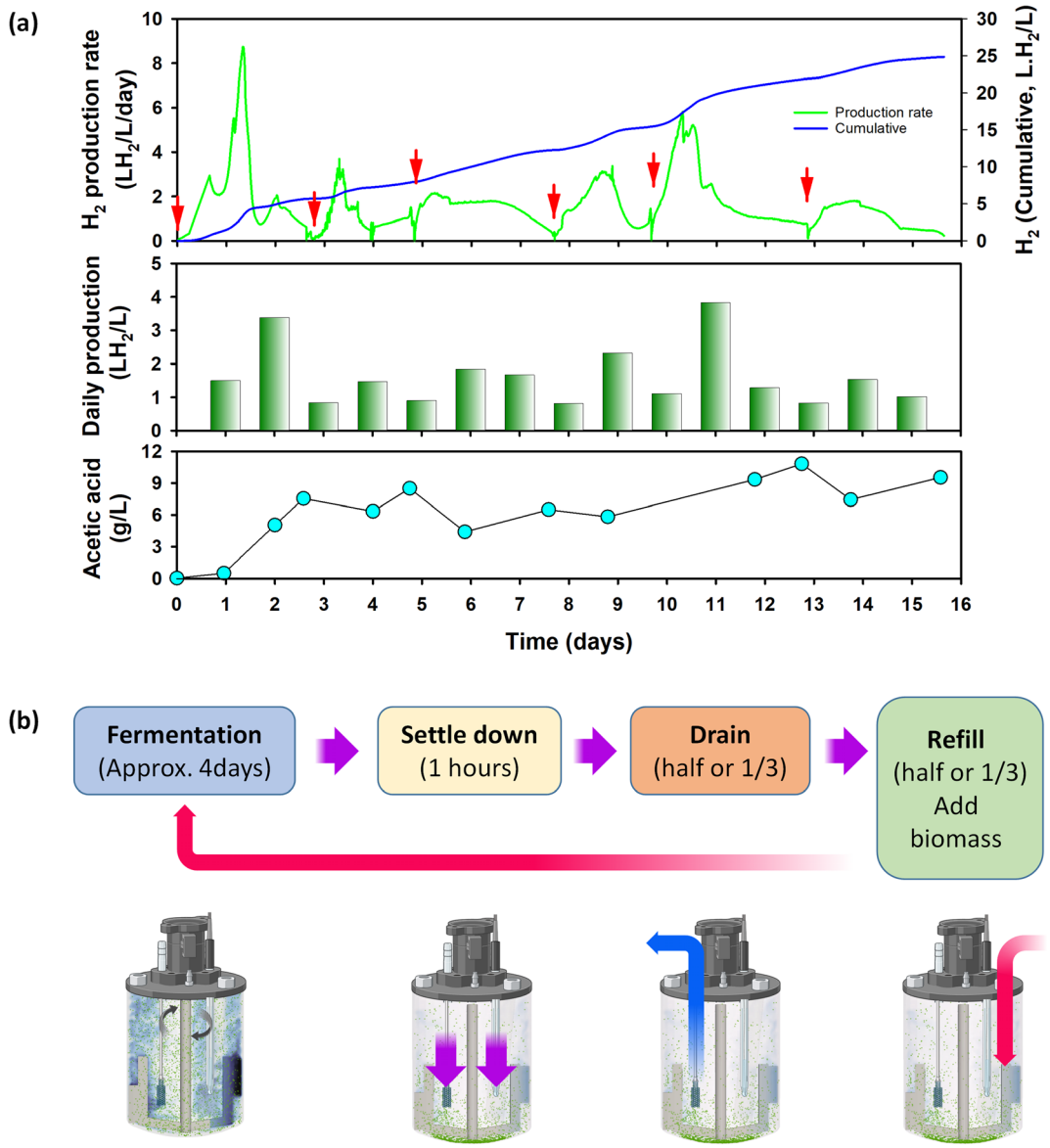

Fig. 6 Hydrogen production in cycling-fed batch operation using the Anchor impeller including daily hydrogen production and accumulated acetate (a). Red arrows indicate bolus additions of 26.7 g L^{-1} DMR-CS. Flow diagram of F–S–D–RF processing for cycling-fed-batch operation process (b).

process differs from general fed-batch operation in that the biomass is allowed to settle, with the supernatant decanted every 2–3 days to control accumulation of toxic by-products. New biomass is then added to repeat the cycle, enabling high flux of solids through the bioreactor while maintaining moderate culture viscosity. Substantial *C. thermocellum* biomass settles with the residual lignin during each decant step, preventing washout. Sequencing fed-batch operation was designed to begin with an initial concentration of 26.6 g L^{-1} DMR-CS, known from batch experimentation to provide maximum hydrogen yields. Following that, the F–S–D–RF cycle was repeated five times: at 3, 5, 8, 10, and 13 days, with 26.7 g L^{-1} of biomass supplied at each cycle and half the media decanted and replaced. In total, 160 g L^{-1} DMR-CS was supplied over the course of the experiment. The cycle period was determined *via* real-time *ex situ* analysis by HPLC, with acetate accumulation used as a deciding parameter to maintain concentrations below 10 g L^{-1}. As a result, hydrogen was continuously produced for 16 days with total accumulated hydrogen production of 24.87 L H_2 L^{-1}, more than 4-fold higher than was achieved in end-batch (Fig. 6). Average daily hydrogen production was approximately 1.50 L H_2 L^{-1} day^{-1}, with a hydrogen yield of 1.615 H_2 mol mol^{-1} total sugars, matching our best results with Avicel and DMR-CS in batch conditions. At the conclusion of the experiment, biomass solubilization efficiency was analyzed, revealing solubilization of 135.0 g L^{-1} DMR-CS, 84.4% of the total supplied. Glucan and xylan consumption was 79.25 g L^{-1} and 25.49 g L^{-1}, respectively, corres-

Table 1 Comparison of the biohydrogen production *via* dark fermentation, comparing previously reported conditions and production values to this study

Strains	Feed stock	Pretreatment	Size (L L^{-1})	Condition (temp, rpm, pH)	Operation	H_2 production (L H_2 L^{-1})	Max H_2 yield	Ref.
Thermoanaerobacterium thermosaccharolyticum W16	Hydrolysate from corn stover	Milled corn stover 2–10 mm Acid hydrolysis	0.05/ 0.1	60 °C, 150 rpm by shaker	Batch	3.31	2.24 mol H_2 mol^{-1} glucose	Cao *et al.* (2009)[19]
Clostridium butyricum DSM 10702	Glucose		0.03/ 0.06	37 °C, 150 rpm by shaker, pH 6.8	Batch	1.57	3.1 mol H_2 mol^{-1} glucose	Hu *et al.* (2013)[64]
Clostridium sp. FS3	Raw corn stalk	Milled, 40 mesh screen	0.05/ 0.14	36 °C, 120 rpm by shaker, pH 7.8	Batch	—	92.9 ml H_2 g^{-1}-corn stalk	Song *et al.* (2014)[65]
Clostridium acetobutylicum ATCC 824	Sugarcane molasses	Acid hydrolysis	0.97/1	30 °C, 100 rpm by stir, pH 6.2	Batch	—	2.83 mol H_2 mol^{-1} glucose	Hassan *et al.* (2015)[18]
Anaerobic digester sludge	Hydrolysate from Rice Husk	Acid hydrolysis	0.04/ 0.1	35 °C, 150 rpm by shaker, pH 7.7	Batch	2.76 ± 0.13	1.96 ± 0.09 mol H_2 mol^{-1} total sugar	Gonzales *et al.* (2016)[20]
Hydrogen pilot plant sludge	Hydrolysate from Sugarcane	Acid hydrolysis	0.1 0.2	37 °C, 150 rpm by shaker	Batch	6.98	—	Sangyoka *et al.* (2016)[66]
Clostridium thermocellum ATCC 27405	Hydrolysate from Sugarcane	Pretreated with NH_4OH–H_2O_2, and two-step acid hydrolysis	0.08/ 0.12	55 °C, 150 rpm by shaker	Batch	25.6 mmol L^{-1}	—	Cheng *et al.* (2016)[67]
E. coli WDHL	Hydrolysate from Wheat straw	Milled >40 mesh Acid hydrolyzed	1/1	31 °C, 175 rpm by stir	Batch	3.28	6.25 mmol H_2 g^{-1} TRS (total reducing sugars)	Lopez-Hidalgo *et al.* (2017)[68]
Clostridium thermocellum DSM 1313 Δhpt	Avicel		2/4.25	60 °C, 60 rpm by stir, pH 7	Batch	74.6 ± 6.7 mmol L^{-1}	1.21 ± 0.14 mmol $mmol^{-1}$ hexose	Singer *et al.* (2018)[69]
Clostridium lentocellum	Cassava residues	Chipped and screened to 10–25 mm	0.05/ 0.1	37 °C, pH 7.0	Batch	—	5.42 mmol H_2 g^{-1} CMC (carboxymethylcellulose)	Zhang *et al.* (2019)[34]
Clostridium butyricum TM-9A	Molasses from sugarcane black strap		9/13.5	37 °C, 80 rpm, pH 8	Batch	1.63	3.34 mol H_2 mol^{-1} synthetic glucose	RamKumar *et al.* (2021)[70]
Clostridium thermocellum KJC Bxint	Corn stover	Deacetylation and mechanical refining (DMR)	0.4/0.5	55 °C150–170 rpm by anchor impeller, pH 7	Batch	≈2.7	≈1.8 mol H_2 mol^{-1} saccharide	Chou *et al.* (2024)[17]
Clostridium thermocellum 7072	Cornstalk	Milled <1 mm powder	6.5/10, 60/100 CSTR	55 °C, 100 rpm by stir, pH 6.4	CSTR	1.07 0.94	58.3 mL of H_2/g 61.4 mL of H_2 g^{-1} cornstalk	Cheng *et al.* (2011)[35]
Clostridium thermocellum ATCC 27405	α-Cellulose	—	5/15	60 °C, 75 rpm by an axial flow impellor, pH 7.2	Continuous	56.6 ml h^{-1} (over 3000 h)	1.65 mol H_2 mol^{-1} hexose	Magnusson *et al.* (2008)[12]
Clostridium acetobutylicum ATCC 824	Glucose	—	2/2.5	37 °C, 200 rpm agitation, pH 5.5	Continuous	6.10 (over 600 h)	2.39 mol of H_2 mol^{-1} glucose	Guerrero *et al.* (2021)[71]
Clostridium thermocellum KJC 19-9	Avicel	—	1.5/2	60 °C150 rpm by anchor impeller, pH 7	Batch	6.83 ± 0.09	1.73 mol H_2 mol^{-1} glucose	This study
Clostridium thermocellum KJC 19-9	Corn stover	Deacetylation and mechanical refining (DMR)	1.5/2	60 °C150 rpm by anchor impeller, pH 7	Batch	4.15 ± 0.21	1.62 mol H_2 mol^{-1} total sugar (cellulose, xylose)	This study
Clostridium thermocellum KJC 19-9	Corn stover	Deacetylation and mechanical refining (DMR)	1.5/2	60 °C100 rpm by anchor impeller, pH 7	Sequencing fed-batch	24.87 (over 380 h)	1.61 mol H_2 mol^{-1} total sugar (cellulose, xylose)	This study

ponding to solubilization efficiencies of 94.87 and 96.87% (Fig. S9).

The F–S–D–RF cycle proved successful for long-term operation, achieving a molar hydrogen production yield comparable to batch operation despite having a solid biomass loading six times higher. Use of the acetate concentration as a parameter to adjust the F–S–D–RF cycle duration demonstrates that long-term hydrogen production is possible with the utilization of supplied DMR-CS biomass under simple algorithmic control. Furthermore, this result confirms that while effective mixing and hydrogen removal is a necessary prerequisite for process intensification in lignocellulosic dark fermentation, in a well-mixed system accumulated acetate and other by-products are the primary barrier limiting continuous operation. These metabolites must therefore be addressed *via* continuous removal to maximize hydrogen flux.

4. Context and implications

While a large number of studies conducted over the last decade have focused on utilizing lignocellulosic biomass *via* dark fermentation, the majority of studies primarily employed either saccharified hydrolysate from pretreated solid biomass or insoluble Avicel biomass for hydrogen production in lab-scale reactors (Table 1). Avicel, a purified microcrystalline cellulose, is useful as a model feedstock for small-scale studies, but the purification process is costly and the end product is not reflective of less refined feedstocks, particularly at high solids loadings as underscored by the results of this study. Lignocellulosic hydrolysates are readily fermentable, but the enzyme cocktails and solid–liquid separation process used to generate hydrolysate from pretreated biomass impose significant costs when compared to CBP. In this study, we validate the potential to match biomass-to-biohydrogen rates and yields achieved at small scales, over short time scales, and with model or saccharified feedstocks, while using unsaccharified feedstocks in long-term, high-intensity operation. This process directly utilizes DMR-CS, a pretreated biomass feedstock with no further processing, as a cost-effective real-world feedstock for biohydrogen production. Both simulation and real-world demonstrations establish that use of customized high-solids mixing geometries can overcome rheological limitations and enhance hydrogen production from solid biomass, eliminating the need for upstream hydrolysis. For well mixed systems with effective hydrolysis, accumulation of soluble metabolites limits reaction progress. A new sequencing fed-batch operation strategy, the F–S–D–RF cycle, couples high solids mixing, acetate removal with simple algorithmic control, and cell retention to enable successful long-term hydrogen production with high biomass flux and high conversion efficiency.

5. Conclusions

In this study, we developed a novel bioreactor system optimized for biohydrogen production from high solid lignocellulosic biomass fermentation using *Clostridium thermocellum* KJC 19-9 in a 2 L bioreactor. Homogeneous mixing of insoluble biomass was crucial, and this behavior was analyzed through CFD simulation. The Anchor impeller was predicted to provide higher mixing velocity under high solid biomass conditions. Indeed, the Anchor impeller significantly enhanced hydrogen production and biomass solubilization compared to the Rushton impeller, achieving a hydrogen production yield comparable to that obtained with Avicel (purified cellulose) with DMR-pretreated corn stover by reaching 1.63 mol H_2 per mol of total sugars contained in glucan and xylan. While improved mixing enhanced hydrogen production and biomass saccharification, increased hydrogen production was accompanied by accumulation of acetate and other metabolites, impeding continuous hydrogen production despite continuous biomass supply. To address this, we implemented a new fed-batch operation strategy to mitigate the accumulation of by-products and extend long-term operation for continuous hydrogen production. Using the F–S–D–RF sequencing fed-batch operation, biohydrogen from lignocellulosic biomass was continuously produced at an average rate of 1.5 L H_2 L^{-1} d^{-1} over 16 days, resulting in a total output of 24.87 L H_2 L^{-1} in the 2 L bioreactor. This study demonstrates that the combination of a high solid biomass reactor equipped with an Anchor impeller and an optimized operation strategy can maximize hydrogen production from lignocellulosic biomass. Additionally, it provides a simple, broadly applicable, and low-cost strategy for long-term operation, paving the way for future commercial applications.

Conflicts of interest

Authors declare no competing interests.

Data availability

Complete primary data for this article, including full batch records and data logs for all reported fermentation experiments, is available at the following source: Song, Young Eun; Kim, Changman; Rachbauer, Lydia *et al.* (2025). Maximizing long-term biohydrogen production with Clostridium thermocellum in high solids lignocellulosic biomass fermentations [Dataset]. Dryad. https://doi.org/10.5061/dryad.3bk3j9kxr

Supplementary information (SI) is available. See DOI: https://doi.org/10.1039/d5gc03052h.

Acknowledgements

This work authored in part by the Lawrence Berkeley National Laboratory and by the National Renewable Energy Laboratory (NREL), operated by Alliance for Sustainable Energy, LLC, for the U.S. Department of Energy (DOE) under Contract No. DE-AC36-08GO28308. Funding was provided by U.S.

Department of Energy Office of Energy Efficiency Renewable Energy Hydrogen and Fuel Cell Technologies Office (FOA DE-LC-000L062). The views expressed in the article do not necessarily represent the views of the DOE or the U.S. Government. The U.S. Government retains and the publisher, by accepting the article for publication, acknowledges that the U.S. Government retains a nonexclusive, paid-up, irrevocable, worldwide license to publish or reproduce the published form of this work, or allow others to do so, for U.S. Government purposes.

References

1 T. Veziro and F. Barbir, *Int. J. Hydrogen Energy*, 1992, **17**, 391–404.
2 I. Dincer and C. Acar, *Int. J. Hydrogen Energy*, 2015, **40**, 11094–11111.
3 IEA, *Global Hydrogen Review 2021*, 2021.
4 P. Parthasarathy and K. S. Narayanan, *Renewable Energy*, 2014, **66**, 570–579.
5 Y.-C. Li, Y.-F. Liu, C.-Y. Chu, P.-L. Chang, C.-W. Hsu, P.-J. Lin and S.-Y. Wu, *Int. J. Hydrogen Energy*, 2012, **37**, 15704–15710.
6 W. Xiong, P. P. Lin, L. Magnusson, L. Warner, J. C. Liao, P.-C. Maness and K. J. Chou, *Proc. Natl. Acad. Sci. U. S. A.*, 2016, **113**, 13180–13185.
7 D. Beri, C. D. Herring, S. Blahova, S. Poudel, R. J. Giannone, R. L. Hettich and L. R. Lynd, *Biotechnol. Biofuels*, 2021, **14**, 24.
8 N. Yutin and M. Y. Galperin, *Environ. Microbiol.*, 2013, **15**, 2631–2641.
9 Y. Nataf, L. Bahari, H. Kahel-Raifer, I. Borovok, R. Lamed, E. A. Bayer, A. L. Sonenshein and Y. Shoham, *Proc. Natl. Acad. Sci. U. S. A.*, 2010, **107**, 18646–18651.
10 Q. An, J.-R. Cheng, Y.-T. Wang and M.-J. Zhu, *Renewable Energy*, 2020, **148**, 214–222.
11 J. Wang and Y. Yin, *Int. J. Hydrogen Energy*, 2021, **46**, 34599–34625.
12 L. Magnusson, N. Cicek, R. Sparling and D. Levin, *Biotechnol. Bioeng.*, 2009, **102**, 759–766.
13 R. Zagrodnik, *Int. J. Hydrogen Energy*, 2022, **47**(84), 35635–35640.
14 E. Elbeshbishy, B. R. Dhar, G. Nakhla and H.-S. Lee, *Renewable Sustainable Energy Rev.*, 2017, **79**, 656–668.
15 S. K. Bhatia, S. S. Jagtap, A. A. Bedekar, R. K. Bhatia, K. Rajendran, A. Pugazhendhi, C. V. Rao, A. E. Atabani, G. Kumar and Y.-H. Yang, *Sci. Total Environ.*, 2021, **765**, 144429.
16 C. R. Carere, T. Rydzak, N. Cicek, D. B. Levin and R. Sparling, *Appl. Microbiol. Biotechnol.*, 2014, **98**, 2829–2840.
17 K. J. Chou, T. Croft, S. D. Hebdon, L. R. Magnusson, W. Xiong, L. H. Reyes, X. Chen, E. J. Miller, D. M. Riley, S. Dupuis, K. A. Laramore, L. M. Keller, D. Winkelman and P.-C. Maness, *Metab. Eng.*, 2024, **83**, 193–205.
18 S. H. Hassan and F. M. Morsy, *Enzyme Microb. Technol.*, 2015, **81**, 56–62.
19 G. Cao, N. Ren, A. Wang, D.-J. Lee, W. Guo, B. Liu, Y. Feng and Q. Zhao, *Int. J. Hydrogen Energy*, 2009, **34**, 7182–7188.
20 R. R. Gonzales, P. Sivagurunathan and S.-H. Kim, *Int. J. Hydrogen Energy*, 2016, **41**, 21678–21684.
21 J. Sun, L. Zhang and K.-C. Loh, *Bioresour. Bioprocess.*, 2021, **8**, 1–21.
22 K. Goria, H. M. Singh, A. Singh, R. Kothari and V. V. Tyagi, *Int. J. Hydrogen Energy*, 2024, **52**, 127–151.
23 S. Dahiya, S. Chatterjee, O. Sarkar and S. V. Mohan, *Bioresour. Technol.*, 2021, **321**, 124354.
24 D. Nagarajan, D.-J. Lee and J.-S. Chang, *Int. J. Hydrogen Energy*, 2019, **44**, 14362–14379.
25 J. F. Soares, T. C. Confortin, I. Todero, F. D. Mayer and M. A. Mazutti, *Renewable Sustainable Energy Rev.*, 2020, **117**, 109484.
26 Preethi, T. M. M. Usman, J. Rajesh Banu, M. Gunasekaran and G. Kumar, *Bioresour. Technol. Rep.*, 2019, **7**, 100287.
27 T. Jarunglumlert, C. Prommuak, N. Putmai and P. Pavasant, *Int. J. Hydrogen Energy*, 2018, **43**, 634–648.
28 O. Sarkar, R. Katakojwala and S. V. Mohan, *Green Chem.*, 2021, **23**, 561–574.
29 D. B. Levin, R. Islam, N. Cicek and R. Sparling, *Int. J. Hydrogen Energy*, 2006, **31**, 1496–1503.
30 Q.-Q. Tian, L. Liang and M.-J. Zhu, *Bioresour. Technol.*, 2015, **197**, 422–428.
31 D. Humbird, A. Mohagheghi, N. Dowe and D. J. Schell, *Biotechnol. Prog.*, 2010, **26**, 1245–1251.
32 A. Dutta, N. Dowe, K. N. Ibsen, D. J. Schell and A. Aden, *Biotechnol. Prog.*, 2010, **26**, 64–72.
33 R. A. Thompson and C. T. Trinh, *Biotechnol. Bioeng.*, 2017, **114**, 2592–2604.
34 L. Zhang, Y. Li, X. Liu, N. Ren and J. Ding, *RSC Adv.*, 2019, **9**, 11179–11185.
35 X.-Y. Cheng and C.-Z. Liu, *Energy Fuels*, 2011, **25**, 1714–1720.
36 H. Jørgensen, J. Vibe-Pedersen, J. Larsen and C. Felby, *Biotechnol. Bioeng.*, 2007, **96**, 862–870.
37 D. B. Hodge, M. N. Karim, D. J. Schell and J. D. McMillan, *Bioresour. Technol.*, 2008, **99**, 8940–8948.
38 Q. Qing and C. E. Wyman, *Biotechnol. Biofuels*, 2011, **4**, 18.
39 C. Kim, I. Wolf, C. Dou, L. Magnusson, P.-C. Maness, K. J. Chou, S. Singer and E. Sundstrom, *Chem. Eng. J.*, 2023, **456**, 141028.
40 I. Valdez-Vazquez, R. Sparling, D. Risbey, N. Rinderknecht-Seijas and H. M. Poggi-Varaldo, *Bioresour. Technol.*, 2005, **96**, 1907–1913.
41 W. Xiong, L. H. Reyes, W. E. Michener, P. C. Maness and K. J. Chou, *Biotechnol. Bioeng.*, 2018, **115**, 1755–1763.
42 A. E. Tafur Rangel, T. Croft, A. F. González Barrios, L. H. Reyes, P.-C. Maness and K. J. Chou, *Sci. Rep.*, 2020, **10**, 14517.
43 X. Chen, E. Kuhn, E. W. Jennings, R. Nelson, L. Tao, M. Zhang and M. P. Tucker, *Energy Environ. Sci.*, 2016, **9**, 1237–1245.

44 A. Sluiter, B. Hames, R. Ruiz, C. Scarlata, J. Sluiter and D. Templeton, *Lab. Anal. Proced.*, 2006, **11**, 65–71.
45 A. Sluiter, B. Hames, R. Ruiz, C. Scarlata, J. Sluiter, D. Templeton and D. Crocker, *Lab. Anal. Proced.*, 2008, **1617**, 1–16.
46 J. Yan, O. Oyedeji, J. H. Leal, B. S. Donohoe, T. A. Semelsberger, C. Li, A. N. Hoover, E. Webb, E. A. Bose, Y. Zeng, C. L. Williams, K. D. Schaller, N. Sun, A. E. Ray and D. Tanjore, *ACS Sustainable Chem. Eng.*, 2020, **8**, 8059–8085.
47 B. Liu, Q. Xiao, P. Gao, B. Sunden and F. Fan, *Chem. Eng. Res. Des.*, 2020, **154**, 60–69.
48 Y. Kamla, H. Ameur, A. Karas and M. I. Arab, *Chem. Pap.*, 2020, **74**, 779–785.
49 T. Kinnarinen, M. Shakhanova, E. Hietanen, R. Salmimies, A. Häkkinen and M. Louhi-Kultanen, *Bioresour. Technol.*, 2012, **110**, 405–411.
50 K. E. Kang, D.-P. Chung, Y. Kim, B.-W. Chung and G.-W. Choi, *Fuel*, 2015, **145**, 18–24.
51 L. R. Lynd, *Annu. Rev. Energy Environ.*, 1996, **21**, 403–465.
52 A. Mohagheghi, M. Tucker, K. Grohmann and C. Wyman, *Appl. Biochem. Biotechnol.*, 1992, **33**, 67–81.
53 J. Zhang, D. Chu, J. Huang, Z. Yu, G. Dai and J. Bao, *Biotechnol. Bioeng.*, 2010, **105**, 718–728.
54 T. Y. Nguyen, C. M. Cai, R. Kumar and C. E. Wyman, *Proc. Natl. Acad. Sci. U. S. A.*, 2017, **114**, 11673–11678.
55 M. De Mey, S. De Maeseneire, W. Soetaert and E. Vandamme, *J. Ind. Microbiol. Biotechnol.*, 2007, **34**, 689–700.
56 S. B. Roberts, C. M. Gowen, J. P. Brooks and S. S. Fong, *BMC Syst. Biol.*, 2010, **4**, 31.
57 J. G. Koendjbiharie, K. Wiersma and R. V. Kranenburg, *Appl. Environ. Microbiol.*, 2018, **84**, e00363–e00318.
58 D. G. Olson, M. Hörl, T. Fuhrer, J. Cui, J. Zhou, M. I. Maloney, D. Amador-Noguez, L. Tian, U. Sauer and L. R. Lynd, *Metab. Eng.*, 2017, **39**, 169–180.
59 C. D. Herring, P. G. Thorne and L. R. Lynd, *Appl. Microbiol. Biotechnol.*, 2016, **100**, 2907–2915.
60 J. Gu, Q. Qiu, Y. Yu, X. Sun, K. Tian, M. Chang, Y. Wang, F. Zhang and H. Huo, *Biotechnol. Biofuels Bioprod.*, 2024, **17**, 2.
61 J. Ralph, *Phytochem. Rev.*, 2010, **9**, 65–83.
62 D. M. de Oliveira, A. Finger-Teixeira, T. Rodrigues Mota, V. H. Salvador, F. C. Moreira-Vilar, H. B. Correa Molinari, R. A. Craig Mitchell, R. Marchiosi, O. Ferrarese-Filho and W. Dantas dos Santos, *Plant Biotechnol. J.*, 2015, **13**, 1224–1232.
63 G. Wang and D. I. Wang, *Appl. Environ. Microbiol.*, 1984, **47**, 294–298.
64 C. C. Hu, A. Giannis, C.-L. Chen, W. Qi and J.-Y. Wang, *Int. J. Hydrogen Energy*, 2013, **38**, 15686–15692.
65 Z.-X. Song, X.-H. Li, W.-W. Li, Y.-X. Bai, Y.-T. Fan and H.-W. Hou, *Bioresour. Technol.*, 2014, **157**, 91–97.
66 S. Sangyoka, A. Reungsang and C.-Y. Lin, *Sustainable Environ. Res.*, 2016, **26**, 235–242.
67 J.-R. Cheng and M.-J. Zhu, *Biotechnol. Bioprocess Eng.*, 2016, **21**, 87–94.
68 A. M. Lopez-Hidalgo, A. Sánchez and A. De León-Rodríguez, *Fuel*, 2017, **188**, 19–27.
69 S. Singer, L. Magnusson, D. Hou, J. Lo, P.-C. Maness and Z. J. Ren, *Environ. Sci.: Water Res. Technol.*, 2018, **4**, 1771–1782.
70 N. RamKumar, P. D. Anupama, T. Nayak and S. Subudhi, *Renewable Energy*, 2021, **170**, 1178–1185.
71 K. Guerrero, R. Gallardo, I. Paredes, J. Quintero, S. Mau, R. Conejeros, J. C. Gentina and G. Aroca, *Int. J. Hydrogen Energy*, 2021, **46**, 5100–5111.